ATLANTIS PRESS
Atlantis Studies in Uncertainty Modelling, volume 3
Joint Proceedings of the 19th World Congress of the International Fuzzy Systems Association (IFSA), the 12th Conference of the European Society for Fuzzy Logic and Technology (EUSFLAT), and the 11th International Summer School on Aggregation Operators (AGOP)

Some Approaches Based on Interval-Valued Images and $\mathbb{L}$-Fuzzy Mathematical Morphology for Segmenting Images Reconstructed from Noisy Sinograms

Peter Sussner [a] and **Lisbeth Corbacho Carazas** [b] and **Eduardo X. Miqueles** [c]
[a] Dept. of Applied Mathematics, University of Campinas, Campinas, SP, Brazil, sussner@ime.unicamp.br
[b] Dept. of Applied Mathematics, University of Campinas, Campinas, SP, Brazil, ra162526@ime.unicamp.br
[c] Brazilian Synchrotron Light Laboratory, CNPEM, Campinas, SP, Brazil, eduardo.miqueles@lnls.br

Abstract

Two-dimensional image reconstruction from projections is a well known research field with different applications and using different sources, e.g., varying from medical imaging to a synchrotron laboratory. In the mathematical sense, we are looking for a two dimensional piecewise function with compact support for which a set of signals - the measurements, so called projections or sinograms - are known *a priori*. After solving the corresponding inverse problem using an appropriate numerical scheme, a collection of reconstructed (gray-scale) images are provided for the final user for further analysis. In practice, the sinogram is often affected by various source of noise which lead to artefacts in the reconstructed images.

In this paper, we first convert the resulting gray-scale image that can be viewed as an $\mathbb{L}$-fuzzy set, where $\mathbb{L}$ is a finite chain, into an interval-valued image whose values are non-empty, closed intervals of $\mathbb{L}$, so as to express the uncertainty about its values. Subsequently, we apply four approaches of morphological image segmentation, all of which make use of the interval values of the image. Each of these approaches employs some type of morphological gradient and the watershed algorithm. We only consider transmission sinograms for this paper, as emission problems are beyond the scope of this paper.

Keywords: Image reconstruction, Signal noise, Fuzzy and interval-valued fuzzy mathematical morphology, Morphological gradient, Image segmentation.

1 Introduction

With some notable exceptions [3, 27], fuzzy mathematical morphology (FMM) is generally viewed as a successful approach to gray-scale image processing [6]. In fact, operators of fuzzy logic have proven to be valuable tools for various tasks of gray-scale morphological image processing and computer vision including edge detection, image segmentation, and pattern recognition. The main reasons why it was possible to formulate morphological image filters using connectives of fuzzy logic are twofold:

1. Gray-scale images can be modelled as fuzzy sets;
2. Both fuzzy logic and mathematical morphology are deeply rooted in lattice theory.

However, when expressing a gray-scale image as a fuzzy set by simply normalizing its values so as to yield the value set $[0, 1]$, one refrains from using fuzzy set theory as a model for uncertainty, vagueness, or imprecision. If the objective is to model uncertainty, vagueness, or imprecision regarding the pixel values of a gray-scale image, one may choose to model an image as an extended fuzzy set. For instance, Nachtegael et al. modelled the numerical and spatial uncertainty due to image capture using interval-valued images [24].

In this paper, we are faced with uncertainty regarding the pixel values of gray-scale images that were reconstructed from a noisy sinogram using an image reconstruction algorithm. Since actual medical images are hard to come by, we performed experiments using a phantom that appeared in several articles of the medical image processing literature [22]. Hence, we decided to use simulated projections, introduce Poisson noise into the sinogram and apply the FBP algorithm to generate an approximate reconstructed image.

More precisely, considering the two-dimensional tomographic problem, we are looking for a compactly

supported 2D function $(x,y) \mapsto f(x,y)$ using a noisy sinogram $(t,\theta) \mapsto p(t,\theta)$ defined as the Radon transform of f,

$$p(t,\theta) = \int_R f(t\cos\theta - s\sin\theta, t\sin\theta + s\cos\theta)\mathrm{d}s. \quad (1)$$

Here, the sinogram p is theoretically determined by Poisson photon counting measurements I and I_0 coming from the experimental setup, i.e., $p = -\log(I/I_0)$. Several uncertainties arise when we restore f from p, but for the discussion in this paper, two of them are important to describe:

1. In practice, the function p is not an ideal Radon transform due to variables beyond the scope of this work such as photon intensity, alignment, dose, among others. Hence, every mathematical framework for inversion has to consider p as the best approximation of a sinogram [4];
2. There exist a class of statistical reconstruction methods that are able to recover f using I, I_0 as input, usually providing better results than others using p as input. Their are computationally expensive if compared to analytical strategies using p, e.g., the classical filtered backprojection algorithm (FBP) [25].

The FBP algorithm, which was the main source for inversion used in this paper, provide a good reconstructed image whenever the number of measured angles is large and p is good approximation for a sinogram.

Assuming that we have no a priori knowledge regarding the corruptions of the reconstructed image, we expressed the aforementioned uncertainty in terms of an interval-valued image. For each reconstructed image, we generate two interval-valued images. The upper and lower bounds of the first one are respectively given by a discrete fuzzy morphological closing and a a discrete fuzzy morphological opening of the image [6]. The upper and lower bounds of the second one are respectively given by the maximum and minimum values of a discrete fuzzy morphological open/close and close/open filter [13, 12]. Then we adopt two different strategies: The first one consists in computing the image whose values are given by the centers of the intervals, which amounts to preordering the intervals using an h-order [14], before processing it further using a fuzzy morphological gradient and a watershed transform [20]. The second strategy includes the computation of a morphological gradient using interval-valued fuzzy morphological operators [24, 30, 31].

The paper is organized as follows. Section 2 briefly reviews some important notions of lattice theory and mathematical morphology. Section 3 explains a general image segmentation methodology based on mathematical morphology as well as the four approaches including some relevant details and modifications considered in this paper. Section 4 describes some experimental results that we obtained by using the aforementioned fuzzy and interval-valued fuzzy morphological approaches in order to segment phantom images that we reconstructed from corrupted sinograms. We finish with some concluding remarks.

2 Some Relevant Concepts of Lattice Theory and Mathematical Morphology

Mathematical morphology offers a wide range of tools for image processing and image understanding. Its theoretical foundations lie in lattice theory and especially complete lattices have turned out to be extremely important in this context [18].

2.1 A Few Notions of Lattice Theory and Mathematical Morphology on Complete Lattices

A reflexive and transitive binary relation "$\leq$" on a non-empty set $\mathbb{P}$ is called a *preorder*. If "$\leq$" is also antisymmetric, then one speaks of a *partial order* and $(\mathbb{P},\leq)$ is called a *partially ordered set* or *poset* [15]. For simplicity, one often writes $\mathbb{P}$ instead of $(\mathbb{P},\leq)$. If X is any non-empty set and $\mathbb{P}$ is a poset, then a mapping $h : X \to \mathbb{P}$ can be used to equip X with the following preorder $\preceq_h$, called *h-order* [14]:

$$x \preceq_h y \Leftrightarrow h(x) \leq h(y). \quad (2)$$

The *closed interval* $[a,b] \subseteq \mathbb{P}$ is defined as the set $\{x \,|\, a \leq x \leq b\}$. For any poset $\mathbb{P}$, a partial order on the direct product of n copies, denoted $\mathbb{P}^n$, can be defined using the following rule:

$$(x_1,\ldots,x_n) \leq (y_1,\ldots,y_n) \iff x_i \leq y_i,\ i = 1,\ldots,n. \quad (3)$$

If $\mathbb{P}$ is a poset and $x \leq y$ or $y \leq x$ for all $x, y \in \mathbb{P}$, then $\leq$ is called a *total* or *linear order* and $(\mathbb{P},\leq)$ is called a *totally ordered set* or a *chain*. The greatest lower bound (g.l.b.) and the least upper bound (l.u.b.) of $M \subseteq \mathbb{P}$ are respectively called the *infimum* and the *supremum* of M are respectively denoted $\bigwedge M$ and $\bigvee M$. If M equals $\{x_i \,|\, i \in I\}$, then the symbols $\bigwedge_{i\in I}$ and $\bigvee_{i\in I}$ replace respectively the symbols $\bigwedge M$ and $\bigvee M$. If $M = \{x,y\}$, then one writes $x \wedge y$ and $x \vee y$ instead of $\bigwedge M$ and $\bigvee M$, respectively. The infimum or the supremum of a subset of a poset does not always exist. If $\bigwedge \mathbb{P}$ and $\bigvee \mathbb{P}$ exist in a poset $\mathbb{P}$, then $\mathbb{P}$ is said to be a *bounded poset*. In this case, the symbols $0_\mathbb{P}$ and $1_\mathbb{P}$ stand respectively for $\bigwedge \mathbb{P}$ and $\bigvee \mathbb{P}$.

If $x \wedge y$ and $x \vee y$ exist for all elements x, y of a poset $\mathbb{P}$, then $(\mathbb{P}, \leq)$ is called a *lattice*. Note that every chain is a lattice. One refers to a lattice $(\mathbb{L}, \leq)$ as a *complete lattice* if $\bigwedge M$ and $\bigvee M$ exist in $\mathbb{L}$ for every $M \subseteq \mathbb{L}$ [2]. The unit interval $[0,1]$ with the usual total order is a complete chain, i.e., a chain that is also a complete lattice. Note that every finite lattice such as $\mathbb{L}_{\frac{1}{n}} = \{0, \frac{1}{n}, \ldots, 1\}$ and $\mathbb{L}_n = \{0, 1, \ldots, n\}$ is complete.

Every complete lattice $\mathbb{L}$ induces a complete lattice of non-empty, closed intervals $\mathbb{I}^*_{\mathbb{L}} = \{[\underline{x}, \overline{x}] \subseteq \mathbb{L} \,|\, \underline{x} \leq \overline{x}\}$ with the partial ordering given by

$$[\underline{x}, \overline{x}] \leq [\underline{y}, \overline{y}] \Leftrightarrow \underline{x} \leq \underline{y} \text{ and } \overline{x} \leq \overline{y}. \tag{4}$$

In the special cases, where $\mathbb{L} = [0,1]$ and $\mathbb{L} = \mathbb{L}_n$, we denote $\mathbb{I}^*_{\mathbb{L}}$ using the symbols $\mathbb{I}^*$ and $\mathbb{I}^*_n$, respectively.

A lattice $(\mathbb{M}, \leq)$ is a called a *sublattice* of $(\mathbb{L}, \leq)$ if $\mathbb{M} \subseteq \mathbb{L}$ and if we have for any $x, y \in \mathbb{M}$ that $x \wedge_{\mathbb{L}} y$ and $x \vee_{\mathbb{L}} y$ are also elements of $\mathbb{M}$. Here, the symbols $\wedge_{\mathbb{L}}$ and $\wedge_{\mathbb{L}}$ indicate that the supremum and the infimum is taken in $\mathbb{L}$. If $\mathbb{M} \subseteq \mathbb{L}$ represent complete lattices, then $\mathbb{M}$ is called a *complete sublattice* of $\mathbb{L}$, if all infima and suprema, taken in $\mathbb{L}$, of subsets of $\mathbb{M}$ are elements of $\mathbb{M}$. For example, we have that the finite chains $\mathbb{L}_{\frac{1}{n}}$ and $\mathbb{L}_n$ are complete sublattices of the complete chains $[0,1]$ and $[0,n]$, respectively.

Any pair consisting of a complete lattice $\mathbb{L}$ and a non-empty set X gives rise to the following complete lattices that are relevant for this paper:

1. $\mathbb{L}^X = \{f : X \to \mathbb{L}\}$ is a a lattice with the following partial order:

$$f \leq g \Leftrightarrow f(x) \leq g(x) \; \forall x \in X. \tag{5}$$

2. The class of all graphs of functions in $\mathbb{L}^X$, denoted using the symbol $\mathscr{F}_{\mathbb{L}}(X)$, is lattice with the partial order given as follows:

$$A \leq B \Leftrightarrow \mu_A \leq \mu_B, \tag{6}$$

for all elements $A = \{(x, \mu_A(x)) \,|\, x \in X\}$ and $B = \{(x, \mu_B(x)) \,|\, x \in X\}$ of $\mathscr{F}_{\mathbb{L}}(X)$. Recall that an element of $\mathscr{F}_{\mathbb{L}}(X)$ is called an $\mathbb{L}$-*fuzzy set* [10]. Hence, $\mathscr{F}_{\mathbb{L}}(X)$ is the class of $\mathbb{L}$-fuzzy sets. Special cases include the following:

   (a) The class of fuzzy sets on $X \neq \emptyset$, denoted $\mathscr{F}(X)$, with the partial ordering of inclusion of fuzzy sets. Note that $\mathscr{F}(X) = \mathscr{F}_{[0,1]}(X)$.
   (b) The class of IV-fuzzy sets on $X \neq \emptyset$, i.e., $\mathscr{F}_{\mathbb{I}^*}(X)$, with the partial order given by Equation 6 for the special case where $(\mathbb{L}, \leq) = (\mathbb{I}^*, \leq)$ (cf. Equation 4).

Recall that $\mu_A \in \mathbb{L}^X$ is referred to as the membership function of A if $A = \{(x, \mu_A(x)) | x \in X\}$. An element of $\mathscr{F}_{\mathbb{L}}(X)$ is called an $\mathbb{L}$-fuzzy set. For simplicity, we write $A(x)$ instead of $\mu_A(x)$.

The complete lattice $\mathscr{F}_{\mathbb{L}}(X)$ can be identified with the complete lattice $\mathbb{L}^X$ by means of a complete lattice isomorphism. In general, one can define a complete lattice isomorphism between complete lattices $\mathbb{L}$ and $\mathbb{M}$ as a bijection $\phi : \mathbb{L} \to \mathbb{M}$ that satisfies the following property for all $x, y \in \mathbb{L}$:

$$x \leq y \Leftrightarrow \phi(x) \leq \phi(y). \tag{7}$$

For every complete lattice $\mathbb{L}$, we have that the mapping given by $A \mapsto \mu_A$ yields a complete lattice isomorphism $\mathscr{F}_{\mathbb{L}}(X) \to \mathbb{L}^X$. Therefore, one says that the complete lattices $\mathscr{F}_{\mathbb{L}}(X)$ and $\mathbb{L}^X$ are isomorphic and one writes $\mathscr{F}_{\mathbb{L}}(X) \simeq \mathbb{L}^X$. We also have that $\mathbb{L}_{\frac{1}{n}} \simeq \mathbb{L}_n$ since mapping $x \in \mathbb{L}_{\frac{1}{n}}$ to $nx \in \mathbb{L}_n$ yields a complete lattice isomorphism that is implicitly used in this paper.

Equation 7 expresses the following fact: If $\phi : \mathbb{L} \to \mathbb{M}$ is a complete lattice isomorphism then both ϕ and ϕ^{-1} are order-preserving or increasing. Recall that a mapping ψ from a poset $\mathbb{P}$ to a poset $\mathbb{Q}$ is called *order-preserving* or *increasing* if the following condition is satisfied for all $x, y \in \mathbb{P}$:

$$x \leq y \Rightarrow \psi(x) \leq \psi(y). \tag{8}$$

The following types of order-preserving mappings are defined in mathematical morphology on complete lattices [17]:

Definition 2.1. Let $\varepsilon, \delta : \mathbb{L} \to \mathbb{M}$, where $\mathbb{L}, \mathbb{M}$ are complete lattices.

1. The mapping ε is called a(n algebraic) erosion if the following equation is satisfied for every index set J and for every set $\{x_j | j \in J\} \subseteq \mathbb{L}$:

$$\varepsilon(\bigwedge_{j \in J} x_j) = \bigwedge_{j \in J} \varepsilon(x_j). \tag{9}$$

2. The mapping δ is a(n algebraic) dilation if the following equation is satisfied for every index set J and for every set $\{x_j | j \in J\} \subseteq \mathbb{L}$:

$$\delta(\bigvee_{j \in J} x_j) = \bigvee_{j \in J} \delta(x_j). \tag{10}$$

Definition 2.2. Let $\delta : \mathbb{L} \to \mathbb{M}$ and $\varepsilon : \mathbb{M} \to \mathbb{L}$. One refers to the pair (ε, δ) as an *adjunction* or says that ε and δ are *adjoint* if only if

$$x \leq \varepsilon(y) \Leftrightarrow \delta(x) \leq y \forall x \in \mathbb{L}, y \in \mathbb{M}. \tag{11}$$

Before summarizing some important facts [16] that we will take advantage of in this paper, let us recall the following definitions:

Definition 2.3. Let $\mathbb{P}$ and $\mathbb{Q}$ be posets. A mapping $\phi : \mathbb{P} \to \mathbb{Q}$ is called

- *idempotent* if $\phi \circ \phi = \mathrm{id}$,
- *extensive* if $x \leq \phi(x)$ for every $x \in \mathbb{P}$,
- *anti-extensive* if $\phi(x) \leq x$ for every $x \in \mathbb{P}$,
- an *opening* if ϕ is increasing, anti-extensive and idempotent,
- a *closing* if ϕ is increasing, extensive and idempotent.

Suppose that ω, κ are respectively an opening and a closing on a poset $\mathbb{P}$. Since ω is anti-extensive and idempotent and κ is extensive and idempotent, we obtain the following relations:

$$\omega = \omega \circ \omega \leq \omega \circ \kappa \leq \kappa \circ \kappa = \kappa, \tag{12}$$

$$\omega = \omega \circ \omega \leq \kappa \circ \omega \leq \kappa \circ \kappa = \kappa. \tag{13}$$

Thus, the following equation holds true for the compositions of an opening and a closing:

$$\omega \leq \omega \circ \kappa, \kappa \circ \omega \leq \kappa. \tag{14}$$

The following theorem shows how to construct openings and closings from erosions and dilations on complete lattices [16]:

Theorem 2.1. Let $\mathbb{L}, \mathbb{M}$ be complete lattices. If $\varepsilon : \mathbb{M} \to \mathbb{L}$ and $\delta : \mathbb{L} \to \mathbb{M}$ are adjoint, then the following statements are valid:

1. The mappings ε and δ are respectively an algebraic erosion and an algebraic dilation.
2. The composition $\delta \circ \varepsilon : \mathbb{M} \to \mathbb{M}$ is an algebraic *opening*.
3. The composition $\varepsilon \circ \delta : \mathbb{L} \to \mathbb{L}$ is an algebraic *closing*.
4. If $\mathbb{L} = \mathbb{M}$, then $\delta(\varepsilon(x)) \leq x \leq \varepsilon(\delta(x))$ for all $x \in \mathbb{L}$.

2.2 $\mathbb{L}$-fuzzy Mathematical morphology

Although the algebraic foundations of mathematical morphology in lattice theory are very general and applicable to a large variety of contexts, the construction of morphological image filters such as opening, closing, open-close filter, morphological gradient, watershed, hit-or-miss transform, that can be used for practical applications, requires the use of so called structuring elements [28]. More precisely, structuring elements can be used to define so called morphological erosions and dilations of images by structuring elements from which morphological image filters can be constructed [18].

To this end, let us consider the framework of $\mathbb{L}$-fuzzy mathematical morphology [31] that generalizes binary, gray-scale, fuzzy, IV-fuzzy, intuitionistic fuzzy, bipolar fuzzy MM, etc. [3, 24, 23, 32]. Here, $\mathbb{L}$ stands for an arbitrary complete lattice that serves as the value set of an image. Note that an image can be represented as an element of $\mathscr{F}_{\mathbb{L}}(X)$ where X is the so called point set of the image. For the purposes of this paper, it suffices to focus on morphological image operators on $\mathscr{F}_{\mathbb{L}}(X)$ (for more general versions, c.f. [19, 29]). The point set is usually a finite subset of $\mathbb{Z}^d$ or $\mathbb{R}^d$. For the purposes of this paper, we may assume from now on that $X = \mathbb{Z}^2$ or any other set that represents an *abelian group* with respect to addition. Considering point sets of images given by a finite subset of $\mathbb{Z}^2$ corresponds to restricting images $\mathbb{Z}^2 \to \mathbb{L}$ to this point set. We prefer to omit a discussion of these technical details in this paper.

In Section 2.1, we reviewed the definitions of erosion and dilation as algebraic operators that commute respectively with the infimum and the supremum operator. In $\mathbb{L}$-fuzzy MM, one defines $\mathbb{L}$-fuzzy (morphological) dilations and erosions in terms of $\mathbb{L}$-fuzzy conjunctions and implications. Definition 2.5 recalls a relatively general way to achieve this goal. First, let us enunciate the definitions of $\mathbb{L}$-fuzzy conjunctions and implications [7]:

Definition 2.4. An increasing mapping $\mathscr{C} : \mathbb{L} \times \mathbb{L} \to \mathbb{L}$ is called an $\mathbb{L}$-*fuzzy conjunction* if $\mathscr{C}(0_{\mathbb{L}}, 0_{\mathbb{L}}) = \mathscr{C}(0_{\mathbb{L}}, 1_{\mathbb{L}}) = \mathscr{C}(1_{\mathbb{L}}, 0_{\mathbb{L}}) = 0_{\mathbb{L}}$ and $\mathscr{C}(1_{\mathbb{L}}, 1_{\mathbb{L}}) = 1_{\mathbb{L}}$. If $\mathscr{C}$ is additionally commutative, associative and satisfies $\mathscr{C}(1_{\mathbb{L}}, x) = x$, then $\mathscr{C}$ is called an $\mathbb{L}$-*fuzzy triangular norm or t-norm*.

A binary operator $\mathscr{I} : \mathbb{L} \times \mathbb{L} \to \mathbb{L}$ is called an $\mathbb{L}$-*fuzzy implication* if $\mathscr{I}(\cdot, z)$ is decreasing for every $z \in \mathbb{L}$, $\mathscr{I}(z, \cdot)$ is increasing for every $z \in \mathbb{L}$ and if $\mathscr{I}(0_{\mathbb{L}}, 0_{\mathbb{L}}) = \mathscr{I}(0_{\mathbb{L}}, 1_{\mathbb{L}}) = \mathscr{I}(1_{\mathbb{L}}, 1_{\mathbb{L}}) = 1_{\mathbb{L}}$ and $\mathscr{I}(1_{\mathbb{L}}, 0_{\mathbb{L}}) = 0_{\mathbb{L}}$.

An $\mathbb{L}$-fuzzy implication $\mathscr{I}$ and conjunction $\mathscr{C}$ on $\mathbb{L}$ are said to be *adjoint* if only if $\mathscr{I}(z, \cdot)$ and $\mathscr{C}(z, \cdot)$ are adjoint for every $z \in \mathbb{L}$.

In the special cases where $\mathbb{L} = [0, 1]$ or $\mathbb{L} = \mathbb{I}$, we obtain fuzzy conjunctions and implications or IV-fuzzy conjunctions and implications, respectively. The fo-

cus of this paper is on value sets of images given by a complete lattice of the form $\mathbb{L}_n = \{0, 1, \ldots, n\}$. In this setting, we may respectively refer to $\mathbb{L}_n$-fuzzy and $\mathbb{I}_n^*$-fuzzy MMs as *discrete fuzzy and interval-valued fuzzy mathematical morphology*.

As mentioned before the complete lattices $\mathbb{L}_n$ and $\mathbb{L}_{\frac{1}{n}}$ are isomorphic under the isomorphism $\phi : \mathbb{L}_{\frac{1}{n}} \to \mathbb{L}_n$ given by $\phi(x) = nx$. Thus, it becomes an easy task to construct $\mathbb{L}_n$-fuzzy conjunctions and implications from fuzzy conjunctions and implications as operators $\mathbb{L}_n \times \mathbb{L}_n \to \mathbb{L}_n$. Let us present some examples below:

$$T_{\mathrm{M}}^n(x,y) = x \wedge y \tag{15}$$

$$T_{\mathrm{nM}}^n(x,y) = \begin{cases} 0 & \text{if } x+y \leq n, \\ x \wedge y & \text{otherwise.} \end{cases} \tag{16}$$

$$I_{\mathrm{GD}}^n(x,y) = \begin{cases} n & \text{if } x \leq y, \\ y & \text{otherwise.} \end{cases} \tag{17}$$

$$I_{\mathrm{FD}}^n(x,y) = \begin{cases} n & \text{if } x \leq y, \\ (n-x) \vee y & \text{otherwise.} \end{cases} \tag{18}$$

For simplicity, let us refer to $T_M^n, T_{\mathrm{nM}}^n, I_{\mathrm{GD}}^n$ and I_{FD}^n as the $\mathbb{L}_n$-fuzzy minimum, nilpotent minimum, Gödel implication, and Fodor implication or simply as the discrete fuzzy minimum, nilpotent minimum, Gödel implication, and Fodor implication, respectively. Note that both the discrete fuzzy minimum and nilpotent minimum are $\mathbb{L}_n$-fuzzy t-norms. Additionally, we have that the pairs $(T_M^n, I_{\mathrm{GD}}^n)$ and $(T_{\mathrm{nM}}^n, I_{\mathrm{FD}}^n)$ form adjunctions. These pairs of $\mathbb{L}_n$-fuzzy morphological operators will be used in Sections 3 and 4 in order to build discrete fuzzy and interval-valued fuzzy morphological erosions and dilations for applications in image processing. For convenience, let us recall the following definition:

Definition 2.5. Let $A, S \in \mathscr{F}_{\mathbb{L}}(X)$ and let $\mathscr{E}_{\mathscr{I}}, \mathscr{D}_{\mathscr{C}} : \mathscr{F}_{\mathbb{L}}(X) \times \mathscr{F}_{\mathbb{L}}(X) \to \mathscr{F}_{\mathbb{L}}(X)$ be defined as follows:

$$\mathscr{E}_{\mathscr{I}}(A,S)(x) = \bigwedge_{y \in X} \mathscr{I}(S(y-x), A(y)) \tag{19}$$

$$\mathscr{D}_{\mathscr{C}}(A,S)(x) = \bigvee_{y \in X} \mathscr{C}(S(x-y), A(y)) \tag{20}$$

The operator $\mathscr{E}_{\mathscr{I}}$ is called the (morphological) $\mathbb{L}$-*fuzzy erosion of the image A by the structuring element (SE) S* and to the operator $\mathscr{D}_{\mathscr{C}}$ as the (morphological) $\mathbb{L}$-*fuzzy dilation of the image A by the structuring element (SE) S*.

The operators $\mathscr{E}_{\mathscr{I}}$ and $\mathscr{D}_{\mathscr{C}}$ are said to be *adjoint* if and only if $\mathscr{E}_{\mathscr{I}}(\cdot, S)$ and $\mathscr{D}_{\mathscr{C}}(\cdot, \bar{S})$ are adjoint for all $S \in \mathscr{F}_{\mathbb{L}}(X)$. Here, the transpose $\bar{S}$ of $S \in \mathscr{F}_{\mathbb{L}}(X)$ is defined by $\bar{S}(x) = S(-x)$ for every $x \in X$.

Generally speaking, a particular approach towards $\mathbb{L}$-fuzzy MM is given by a pair consisting of an $\mathbb{L}$-fuzzy erosion $\mathscr{E}_{\mathscr{I}}$ and an $\mathbb{L}$-fuzzy dilation $\mathscr{D}_{\mathscr{C}}$. One usually employs a pair $(\mathscr{E}_{\mathscr{I}}, \mathscr{D}_{\mathscr{C}})$ such that $\mathscr{I}$ and $\mathscr{C}$ are adjoint since in this case $\mathscr{E}_{\mathscr{I}}$ and $\mathscr{D}_{\mathscr{C}}$ have several useful algebraic properties such as the following [31]:

Theorem 2.2. For any $\mathbb{L}$-fuzzy conjunction $\mathscr{C}$ and any $\mathbb{L}$-fuzzy implication $\mathscr{I}$, we have:

- $\mathscr{E}_{\mathscr{I}}(\cdot, S)$ are algebraic erosions $\forall\ S \in \mathscr{F}_{\mathbb{L}}(X)$ if and only if $\mathscr{I}(\cdot, s)$ are algebraic erosions $\forall\ s \in \mathbb{L}$.
- $\mathscr{D}_{\mathscr{C}}(\cdot, S)$ are algebraic dilations $\forall\ S \in \mathscr{F}_{\mathbb{L}}(X)$ if and only if $\mathscr{C}(\cdot, s)$ are algebraic erosions $\forall\ s \in \mathbb{L}$.
- $\mathscr{I}$ and $\mathscr{C}$ are adjoint if and only if $\mathscr{E}_{\mathscr{I}}$ and $\mathscr{D}_{\mathscr{C}}$ are adjoint.

Proposition 2.1. Let $S \in \mathscr{F}_{\mathbb{L}}(X)$ be such that $S(\mathbf{0}) = 1_{\mathbb{L}}$. If $(\mathscr{I}, \mathscr{T})$ is an adjunction consisting of an $\mathbb{L}$-fuzzy implication and an $\mathbb{L}$-fuzzy t-norm, then we have:

$$\mathscr{E}_{\mathscr{I}}(A,S) \leq A \leq \mathscr{D}_{\mathscr{T}}(A,S)\ \forall A \in \mathscr{F}_{\mathbb{L}}(X). \tag{21}$$

Given a structuring element $S \in \mathscr{F}_{\mathbb{L}}(X)$ as well as an $\mathbb{L}$-fuzzy implication $\mathscr{I}$ and an $\mathbb{L}$-fuzzy conjunction $\mathscr{C}$ that are adjoint operators, we infer the following in light of Theorem 2.1: If $\varepsilon = \mathscr{E}_{\mathscr{I}}(\cdot, S)$ and $\delta = \mathscr{D}_{\mathscr{C}}(\cdot, \bar{S})$, then $\delta \circ \varepsilon$ is an algebraic opening and $\varepsilon \circ \delta$ is an algebraic closing $\mathscr{F}_{\mathbb{L}}(X) \to \mathscr{F}_{\mathbb{L}}(X)$. Consequently, we have

$$\delta(\varepsilon(A)) \leq A \leq \varepsilon(\delta(A))\ \forall A \in \mathscr{F}_{\mathbb{L}}(X). \tag{22}$$

Representable $\mathbb{I}_{\mathbb{L}}^*$-fuzzy conjunctions and t-norms [1] can be derived from $\mathbb{L}$-fuzzy conjunctions and t-norms, respectively, as follows:

Definition 2.6. Let C be an $\mathbb{L}$-fuzzy conjunction. The *representable conjunction* with representative C, denoted using the symbol $\mathscr{C}_C^r$ is the $\mathbb{I}_{\mathbb{L}}^*$-fuzzy operators that satisfies the following equation for all $\mathbf{x} = [\underline{x}, \overline{x}]$, $\mathbf{y} = [\underline{y}, \overline{y}] \in \mathbb{I}_{\mathbb{L}}^*$:

$$\mathscr{C}_C^r(\mathbf{x}, \mathbf{y}) = [C(\underline{x}, \underline{y}), C(\overline{x}, \overline{y})]. \tag{23}$$

Evidently, we have that $\mathscr{C}_T^r$ is an $\mathbb{I}_{\mathbb{L}}^*$-fuzzy t-norm if and only if T is an $\mathbb{L}$-fuzzy t-norm in which case we write $\mathscr{C}_T^r$ instead of $\mathscr{T}_T^r$.

The following proposition arises as a corollary of Theorem 14 of [31]:

Proposition 2.2. Let I and T be respectively be an $\mathbb{L}$-fuzzy implication and an $\mathbb{L}$-fuzzy t-norm, where $\mathbb{L}$ is a complete chain. The following expression yields an $\mathbb{I}^*_{\mathbb{L}}$-fuzzy implication

$$\mathscr{I}_I^R(\mathbf{x},\mathbf{y}) = [I(\underline{x},\underline{y}) \wedge I(\overline{x},\overline{y}), I(\overline{x},\overline{y})]\,. \qquad (24)$$

Furthermore, we have that the operators $\mathscr{I}_I^R$ and $\mathscr{T}_T^r$ are adjoint if only if I and T are adjoint.

3 Image Segmentation Using Discrete Fuzzy and Interval-Valued Fuzzy Mathematical Morphology

One of the most widely known applications of mathematical morphology is image segmentation using the watershed transform [26]. There are several versions of this transform including Vincent's and Soille's immersion algorithm [34] and F. Meyer's topographical distance algorithm [21]. The latter was used in the simulations that were performed in this paper. Usually, one does not apply the watershed transform to the given original gray-scale image but to a so called *morphological gradient* of the image. A morphological gradient image is given by the difference of the closing and the opening of the image [28]. To diminish problems with oversegmentation in the subsequent application of the watershed algorithm, one usually applies the h-minima transform in order to suppress local minima in the gray-scale image, i.e., valleys, whose depth is less than h.

As usual, the gray-scale images in this paper have integer pixel values ranging from 0 to 255. In other words, these gray-scale images can be viewed as $\mathbb{L}_{255}$-fuzzy sets. From now on, let n be 255 and let $\mathscr{F}_n(X)$ stand for $\mathscr{F}_{\mathbb{L}}(X)$, where $\mathbb{L} = \mathbb{L}_{255}$ so as to facilitate the discussions that are still to come.

The computation of the morphological gradient of a given image $A \in \mathscr{F}_n(X)$ requires the application of $\mathbb{L}_n$-fuzzy morphological closing and opening operators that, according to Theorem 2.1., can be constructed via compositions of an erosion and a dilation $\mathscr{F}_n(X) \to \mathscr{F}_n(X)$ that yield an adjunction. By Theorem 2.2, an adjunction consisting of an erosion and a dilation is given by an erosion of the form $\mathscr{E}_{\mathscr{I}}(\cdot,S)$ and a dilation of the form $\mathscr{D}_{\mathscr{C}}(\cdot,S)$, where $\mathscr{I}$ and $\mathscr{C}$ are respectively an $\mathbb{L}_n$-fuzzy implication and an $\mathbb{L}_n$-fuzzy conjunction that are adjoint and where S is some $\mathbb{L}_n$-fuzzy SE. We selected the $\mathbb{L}_n$-fuzzy nilpotent minimum T^n_{nM} and the Fodor implication I^n_{GD} as an adoint pair of $\mathbb{L}_n$-fuzzy operators as well as the $\mathbb{L}_n$-fuzzy SE (invariant) S whose non-zero values are given by the following matrix:

$$S = \begin{pmatrix} 219 & 219 & 219 \\ 219 & 255 & 219 \\ 219 & 219 & 219 \end{pmatrix}. \qquad (25)$$

This is to say that $S(0,0) = 255$ and $S(i,j) = 219$ for all $i,j \in \{-1,0,1\}$ except for $(0,0)$. Our choices of T^n_{nM}, I^n_{GD}, and S were motivated by the fact that, together with the normalized version of S, i.e., $S/255$, the respective fuzzy versions of these operators, i.e., T^1_{nM} and I^1_{GD}, were among the statistically best choices of a fuzzy conjunction-implication pair, found by Gonzalez-Hidalgo et al. [11], for a fuzzy morphological edge detector which depends on a fuzzy morphological gradient. Hereafter, we applied an h-minima transform after determining a suitable parameter h in a training phase.

The experiment illustrated in Figure 1 shows the original uncorrupted image, the image obtained by computing the aforementioned fuzzy morphological gradient followed by the h-minima transform with $h = 4$ and the segmentation produced by the watershed transform.

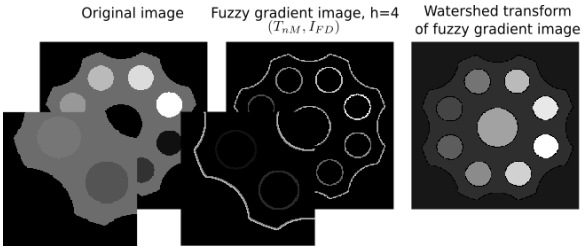

Figure 1: From left to right: Original image, fuzzy morphological gradient followed by the h-minima transform with $h = 4$, segmentation produced by the watershed transform.

The next figure visualizes the same type of experiment. However, the leftmost image was reconstructed on the basis of a sinogram that contains noise drawn from Poisson distributions.

The poor result of the segmentation is clearly visible on the right hand side of Figure 2 (we increased h from 4 to 10 so as to avoid an even poorer segmentation result). One may argue that the pixel values of the reconstructed image are inherently uncertain and that this uncertainty can be taken into account by mapping the image obtained from the reconstruction based on a noisy sinogram to an interval-valued image.

By Theorems 2.1, an interval-valued image is given by $[\omega(A), \kappa(A)] \in \mathscr{F}_{\mathbb{I}^*_n}(X)$, where $\omega = \delta \circ \varepsilon$ and $\kappa = \varepsilon \circ \delta$ for some adjoint $\varepsilon, \delta : \mathscr{F}_n(X) \to \mathscr{F}_n(X)$. As mentioned before, an $\mathbb{L}_n$-fuzzy implication $\mathscr{I}$ and its adjoint $\mathbb{L}_n$-

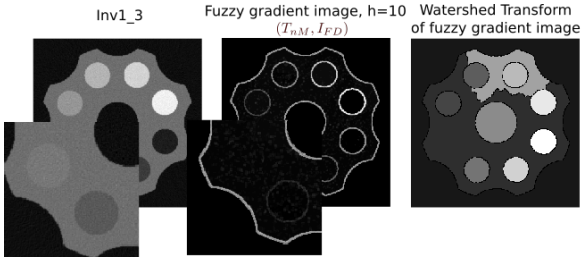

Figure 2: From left to right: Image reconstructed from a noisy sinogram containing Poisson noise, fuzzy morphological gradient followed by the h-minima transform with $h = 10$, segmentation produced by the watershed transform.

fuzzy conjunction $\mathscr{C}$ together with an SE $S \in \mathscr{F}_n(X)$ give rise to an adjunction $(\mathscr{E}_{\mathscr{I}}(\cdot,S), \mathscr{D}_{\mathscr{C}}(\cdot,S))$. We selected the 8-connected disk with radius 1, i.e., a flat 3×3 SE, the $\mathbb{L}_n$-fuzzy minimum T_M^n and its adjoint implication I_{GD}^n because these choices of S, $\mathscr{C}$ and $\mathscr{I}$ do not produce any new pixel values in $\mathscr{D}_{\mathscr{C}}(\mathscr{E}_{\mathscr{I}}(A,S),S)$ and $\mathscr{E}_{\mathscr{I}}(\mathscr{D}_{\mathscr{C}}(A,S),S)$ in comparison to the pixel values of $A \in \mathscr{F}_n(X)$. For simplicity, let $\omega_{\mathrm{GD,M}}^n$ and $\kappa_{\mathrm{M,GD}}^n$ denote respectively the opening and the closing based on I_{FD}^n and T_{nM}^n (recall that morphological openings and closings can be used to reduce dilative and erosive noise, respectively).

To process the image $[\omega_{\mathrm{GD,M}}^n(A), \kappa_{\mathrm{M,GD}}^n(A)] \in \mathscr{F}_{\mathbb{I}_n^*}(X)$ using techniques of mathematical morphology other than interval-valued FMM, one may opt to immediately remove the uncertainty and reduce the lengths of the intervals to 0 by mapping each interval to its center, i.e., mapping the image $[\omega_{\mathrm{GD,M}}^n(A), \kappa_{\mathrm{M,GD}}^n(A)]$ to the arithmetic mean of $\omega_{\mathrm{GD,M}}^n(A)$ and $\kappa_{\mathrm{M,GD}}^n(A)$ which has values in $\mathbb{L}_{\frac{1}{2}}^n = \{0, \frac{1}{2}, 1, \ldots, n\} \simeq \mathbb{L}^{2n}$. Thus, we might as well associate $[\omega_{\mathrm{GD,M}}^n(A), \kappa_{\mathrm{M,GD}}^n(A)] \in \mathscr{F}_{\mathbb{I}_n^*}(X)$ with $\omega_{\mathrm{GD,M}}^n(A) + \kappa_{\mathrm{M,GD}}^n(A) \in \mathbb{L}^{2n}$. Note that this boils down to defining the following h-order in $\mathscr{F}_{\mathbb{I}_n^*}(X)$ (cf. Equation 2):

$$[\underline{A}, \overline{A}] \preceq [\underline{B}, \overline{B}] \Leftrightarrow \underline{A} + \overline{A} \leq \underline{B} + \overline{B}. \tag{26}$$

In the following, let $m = 2n$. We now have image in $\mathscr{F}^m(X)$ at hand, to which operators of $\mathbb{L}^m$-fuzzy MM, in particular the $\mathbb{L}^m$-fuzzy morphological gradient based on T_{nM}^m and I_{FD}^m and using $2S$ as an SE, where S is as in Equation 25, can be applied. Then we executed the same steps as before in order to produce the segmentation. Figure 3 illustrates this procedure.

As an alternative approach, we can deal with the image $[\omega_{\mathrm{GD,M}}^n(A), \kappa_{\mathrm{M,GD}}^n(A)] \in \mathscr{F}_{\mathbb{I}_n^*}(X)$ using operators of $\mathbb{I}_n^*$-fuzzy MM. Specifically, we computed the $\mathbb{I}_n^*$-fuzzy dilation of this image by the SE S given in Equation 25

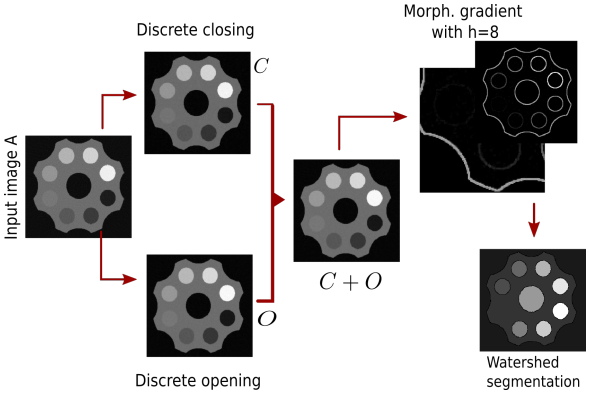

Figure 3: From left to right: Image A reconstructed from noisy sinogram, interval-valued image $[\omega_{\mathrm{GD,M}}^n(A), \kappa_{\mathrm{M,GD}}^n(A)] \in \mathscr{F}_{\mathbb{I}_n^*}(X)$, $\mathbb{L}^m$-fuzzy image $\omega_{\mathrm{GD,M}}^n(A) + \kappa_{\mathrm{M,GD}}^n(A)$, $\mathbb{L}^m$-fuzzy morphological gradient based on T_{nM}^m and I_{FD}^m followed by h-minima transform, watershed segmentation.

based on the representable t-norm $\mathscr{T}_T^r$ for $T = T_{\mathrm{nM}}^n$ and the $\mathbb{I}_n^*$-fuzzy erosion of this image by the SE S given in Equation 25 based on the implication I_I^R for $I = I_{\mathrm{FD}}^n$. For simplicity, let us denote these operators $\mathscr{F}_{\mathbb{I}_n^*}(X) \to \mathscr{F}_{\mathbb{I}_n^*}(X)$ using the symbols $\delta_{\mathrm{nM}}^{r,n}$ and $\varepsilon_{\mathrm{FD}}^{R,n}$. Then, we converted $\delta_{\mathrm{nM}}^{r,n}(A)$ and $\varepsilon_{\mathrm{FD}}^{R,n}(A)$ into elements of $\mathscr{F}^m(X)$ by adding the lower and upper bound images. Afterwards, we computed an $\mathbb{L}^m$-fuzzy morphological gradient in terms of the difference of the two elements of $\mathscr{F}^m(X)$ that we had obtained before. Finally, we applied the h-minima transform and the watershed algorithm. Figure 4 clarifies this methodology.

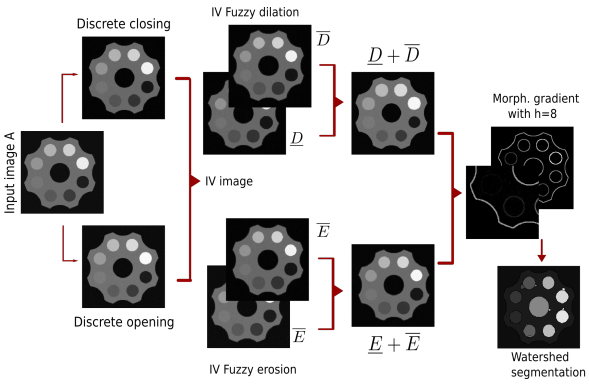

Figure 4: From left to right: Image A reconstructed from noisy sinogram, interval-valued image $[\omega_{\mathrm{GD,M}}^n(A), \kappa_{\mathrm{M,GD}}^n(A)] \in \mathscr{F}_{\mathbb{I}_n^*}(X)$, $\mathbb{I}_n^*$-fuzzy dilation $\delta_{\mathrm{nM}}^{r,n}$ and $\mathbb{I}_n^*$-fuzzy erosion $\varepsilon_{\mathrm{FD}}^{R,n}$, sum of lower and upper bounds in $\mathscr{F}^m(X)$, $\mathbb{L}^m$-fuzzy morpological gradient plus h-minima transform, watershed.

In the last two methods described in this paper, we constructed another interval-valued image in $\mathscr{F}_{\mathbb{I}_n^*}(X)$ instead of $[\omega^n_{\mathrm{GD,M}}(A), \kappa^n_{\mathrm{M,GD}}(A)]$. By Equation 14 and Theorem 2.1, we have the following relation (id^n denoted the identity mapping $\mathscr{F}^n(X) \to \mathscr{F}^n(X)$):

$$\omega^n_{\mathrm{GD,M}} \leq id^n, \omega^n_{\mathrm{GD,M}} \circ \kappa^n_{\mathrm{M,GD}}, \kappa^n_{\mathrm{M,GD}} \circ \omega^n_{\mathrm{GD,M}} \leq \kappa^n_{\mathrm{M,GD}}. \tag{27}$$

Let $\omega\kappa^n_{\mathrm{M,GD}}$ and $\kappa\omega^n_{\mathrm{M,GD}}$ denote $\omega^n_{\mathrm{GD,M}} \circ \kappa^n_{\mathrm{M,GD}}$ and $\kappa^n_{\mathrm{M,GD}} \circ \omega^n_{\mathrm{GD,M}}$, respectively. Note that $\omega\kappa^n_{\mathrm{M,GD}}$ and $\kappa\omega^n_{\mathrm{M,GD}}$ correspond respectively to fuzzy close-open and open-close filters based on T^n_{nM} and I^n_{GD} using a single SE S [13]. In view of Equation 27, it seems reasonable to consider the following interval-valued image

$$[\omega\kappa^n_{\mathrm{M,GD}} \wedge \kappa\omega^n_{\mathrm{M,GD}}, \omega\kappa^n_{\mathrm{M,GD}} \vee \kappa\omega^n_{\mathrm{M,GD}}] \in \mathscr{F}_{\mathbb{I}_n^*}(X). \tag{28}$$

Apart from replacing $[\omega^n_{\mathrm{GD,M}}(A), \kappa^n_{\mathrm{M,GD}}(A)]$ by the image given by Equation 28, we proceeded as described in Figures 3 and 4. Figures 5 and 6 below are meant to clarify these two methodologies.

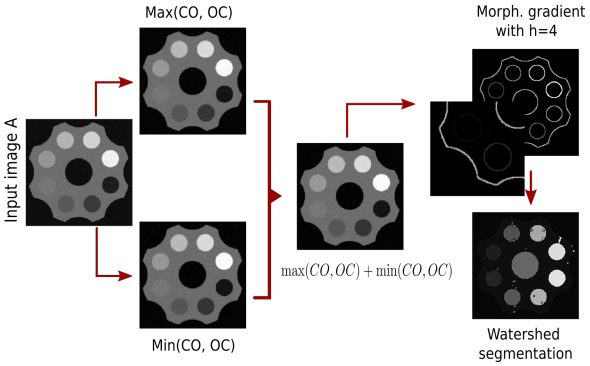

Figure 5: From left to right: Image A reconstructed from noisy sinogram, interval-valued image $[\omega\kappa^n_{\mathrm{M,GD}} \wedge \kappa\omega^n_{\mathrm{M,GD}}, \omega\kappa^n_{\mathrm{M,GD}} \vee \kappa\omega^n_{\mathrm{M,GD}}] \in \mathscr{F}_{\mathbb{I}_n^*}(X)$, transformation to $\mathbb{L}^m$-fuzzy image, $\mathbb{L}^m$-fuzzy morphological gradient based on T^m_{nM} and I^m_{FD} followed by h-minima transform, watershed.

4 Some Experimental Results

Usually, a sinogram is modelled by the Radon transform (a linear operator) for transmission tomography experiments (CT) [25] or its weighted version for emission problems such as PET, SPECT or XFCT [5, 8, 33]. After solving the inverse problem using an appropriate numerical scheme, a collection of reconstructed (gray-scale) images are provided for the final user for further analysis.

Figure 7 displays the uncorrupted sinogram of the phantom used in our simulations [22] before we introduced Poisson type noise.

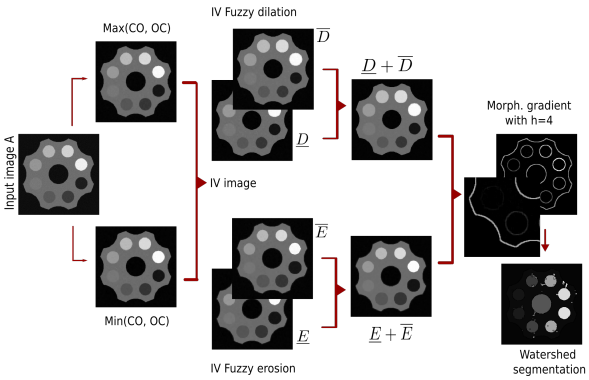

Figure 6: From left to right: Image A reconstructed from noisy sinogram, interval-valued image $[\omega\kappa^n_{\mathrm{M,GD}} \wedge \kappa\omega^n_{\mathrm{M,GD}}, \omega\kappa^n_{\mathrm{M,GD}} \vee \kappa\omega^n_{\mathrm{M,GD}}] \in \mathscr{F}_{\mathbb{I}_n^*}(X)$, $\mathbb{I}_n^*$-fuzzy dilation $\delta^{r,n}_{\mathrm{nM}}$ and $\mathbb{I}_n^*$-fuzzy erosion $\varepsilon^{R,n}_{\mathrm{FD}}$, sum of lower and upper bounds in $\mathscr{F}^m(X)$, $\mathbb{L}^m$-fuzzy morpological gradient plus h-minima transform, watershed.

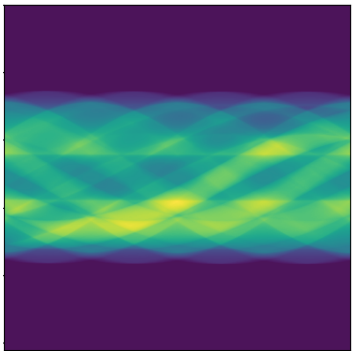

Figure 7: Sinogram of the phantom used in this paper.

Recall that the Poisson distribution is determined by a single paramenter λ which equals both its mean and its variance. The sinogram is given by a 512×512 matrix P corresponding to the photon count. At each position $(i, j) \in 512 \times 512$, we introduced Poisson noise with parameter λ_{ij} according to the following formula:

$$\lambda_{i,j} = \frac{kp_{ij}}{\sum_{i,j=1}^{512} p_{ij}} \tag{29}$$

We used a single constant k, namely $k = 1957945205.4794521$. For the sinogram displayed in Figure 7, the entries p_{ij} sum up to 45355743.06680815.

We employed a training and a testing phase. In the latter, we carried out 50 experiments for each of the methods described in Figures 3 - 6 that we will refer to as

FMG, CO-FMG, CO-IVFMG, OC-CO-FMG and OC-CO-IVFMG. The goal of the training phase consisted in determining a suitable parameter h for the h-minima transform. To this end, we performed 15 experiments for each method and each $h \in \{3,4,\ldots,13\}$, assuming that in the real world the sinograms including the noise they contain are quite similar. We evaluated the values corresponding to a slight modification of the Jaccard index [9], one of the most commonly used metrics in image segmentation.

The Jaccard index JC compares the ground truth (Im_{GT}) and the segmentation result (Im_S) using the following formula:

$$JC = \frac{|Im_{GT} \cap Im_S|}{|Im_{GT} \cup Im_S|} \tag{30}$$

The numerator represents the number of matching pixels and the denominator represents the number of matches and mismatches.

However, as indicated by its name, the watershed algorithm yields the segmentation produced by this algorithm contains watershed lines.

Note that the watershed pixels can neither be classified as matches nor as mismatches. Therefore, we slightly modified the Jaccard index as follows:

$$JC_{\mathrm{m}} = \frac{TP}{FP+FN+TP}. \tag{31}$$

where $TP = |int(Im_S) \cap Im_{GT}|$, $FP = |int(Im_S) \cap (Im_{GT})^c|$, $FN = |(Im_S)^c \cap Im_{GT}|$ and int and $\cdot^c$ stand respectively for the interior and the complement.

Using JC_{m} as a performance measure, the training phase yielded the unique values of h for the h-minima transform that appear in Table 4 below. This table also presents the the mean JC_{m} indexes as well as the standard deviations for each of the five approaches in the testing phase. Figure 8 provides a visual interpretation of the results.

Note that the two methods that are based on the discrete interval images constructed using the close-open and open-close filters exhibited the best performance in our simulations. We suspect that the lengths of the intervals modelling uncertainty in the interval images whose upper and lower bounds are respectively given by morphological closing and opening operators is too large.

5 Concluding Remarks

In this paper, we discussed some approaches for segmenting images that were reconstructed from noisy sinograms. We expressed the uncertainties regarding the values of the reconstructed images using a transformation to an interval-valued image. Then, we proposed two approaches for calculating a morphological gradient, a post-processed version of which can be fed into the watershed algorithm so as to yield a segmentation of the image.

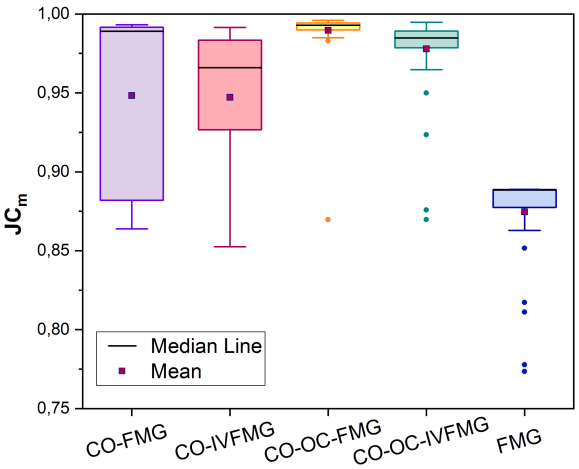

Figure 8: Boxplot for the five methods under consideration.

Method w/ Watershed	h-min.	JC_{m}
FMG	10	0.8746 ± 0.0285
CO-FMG	8	0.9483 ± 0.0541
CO-IVFMG	8	0.9471 ± 0.0453
OC-CO-FMG	4	0.9896 ± 0.0176
OC-CO-IVFMG	4	0.9779 ± 0.0247

Table 1: Average and standard deviations of the JC_{m} values over 50 images for each of the five methods .

Acknowledgement

This work was supported in part by CNPq under grant nos. 315638/2020-6 and 142461/2018-0 and by FAPESP under grants nos. 2018/13657-1 and 2020/09838-0.

References

[1] B. C. Bedregal, H. S. Santos, R. Callejas-Bedregal, A generalized class of T-norms from a categorical point of view, in: 2007 IEEE International Fuzzy Systems Conference, IEEE, London, UK, 2007, pp. 1–6.

[2] G. Birkhoff, Lattice Theory, 3rd Edition, American Mathematical Society, Providence, 1993.

[3] I. Bloch, Mathematical morphology on bipolar fuzzy sets: general algebraic framework, Interna-

tional Journal of Approximate Reasoning 53 (7) (2012) 1031–1060.

[4] T. M. Buzug, Computed tomography, in: Springer Handbook of Medical Technology, Springer, 2011, pp. 311–342.

[5] S.-K. Cheong, B. L. Jones, A. K. Siddiqi, F. Liu, N. Manohar, S. H. Cho, X-ray fluorescence computed tomography (XFCT) imaging of gold nanoparticle-loaded objects using 110 kvp x-rays, Physics in Medicine & Biology 55 (3) (2010) 647.

[6] T.-Q. Deng, H. J. Heijmans, Grey-scale morphology based on fuzzy logic, Journal of Mathematical Imaging and Vision 16 (2) (2002) 155–171.

[7] G. Deschrijver, C. Cornelis, Representability in interval-valued fuzzy set theory, International Journal of Uncertainty, Fuzziness and Knowledge-Based Systems 15 (03) (2007) 345–361.

[8] S. Ganan, D. McClure, Bayesian image analysis: An application to single photon emission tomography, Amer. Statist. Assoc (1985) 12–18.

[9] F. Ge, S. Wang, T. Liu, New benchmark for image segmentation evaluation, J. Electronic Imaging 16 (2007) 033011.

[10] J. Goguen, L-fuzzy sets, Journal of Mathematical Analysis and Applications 18 (1) (1967) 145–174.

[11] M. González-Hidalgo, S. Massanet, A. Mir, D. Ruiz-Aguilera, On the choice of the pair conjunction–implication into the fuzzy morphological edge detector, IEEE Transactions on Fuzzy Systems 23 (4) (2015) 872–884.

[12] M. González-Hidalgo, S. Massanet, J. Torrens, Discrete t-norms in a fuzzy mathematical morphology: Algebraic properties and experimental results, in: Fuzzy Systems (FUZZ), 2010 IEEE Int. Conf. on, IEEE, 2010, pp. 1–8.

[13] M. González-Hidalgo, S. Massanet, A. Mir, D. Ruiz-Aguilera, Improving salt and pepper noise removal using a fuzzy mathematical morphology-based filter, Applied Soft Computing 63 (2018) 167–180.

[14] J. Goutsias, H. J. Heijmans, K. Sivakumar, Morphological operators for image sequences, Computer Vision and Image Understanding 62 (3) (1995) 326–346.

[15] G. A. Grätzer, Lattice Theory: First Concepts and Distributive Lattices, W. H. Freeman, San Francisco, CA, 1971.

[16] H. Heijmans, Mathematical morphology: a geometrical approach in image processing, Nieuw Archief voor Wiskunde 10 (3).

[17] H. Heijmans, C. Ronse, The algebraic basis of mathematical morphology I. dilations and erosions, Computer Vision, Graphics, and Image Processing 50 (3) (1990) 245 – 295.

[18] H. J. Heijmans, Morphological image operators, Advances in Electronics and Electron Physics Suppl., Boston: Academic Press,| c1994.

[19] N. Madrid, M. Ojeda-Aciego, J. Medina, I. Perfilieva, L-fuzzy relational mathematical morphology based on adjoint triples, Inf. Sci. 474 (2019) 75–89.

[20] F. Meyer, Topographic distance and watershed lines, Signal Processing 38 (1) (1994) 113–125.

[21] F. Meyer, S. Beucher, Morphological segmentation, Journal of Visual Communication and Image Representation 1 (1) (1990) 21–45.

[22] E. X. Miqueles, J. Rinkel, F. O'Dowd, J. S. V. Bermúdez, Generalized Titarenko's algorithm for ring artefacts reduction, Journal of Synchrotron Radiation 21 (6) (2014) 1333–1346.

[23] M. Nachtegael, E. E. Kerre, Connections between binary, gray-scale and fuzzy mathematical morphologies, Fuzzy sets and systems 124 (1) (2001) 73–85.

[24] M. Nachtegael, P. Sussner, T. Mélange, E. E. Kerre, On the role of complete lattices in mathematical morphology: From tool to uncertainty model, Information Sciences 181 (10) (2011) 1971–1988.

[25] F. Natterer, The Mathematics of Computerized Tomography, Society for Industrial and Applied Mathematics, USA, 2001.

[26] J. B. Roerdink, A. Meijster, The watershed transform: Definition, algorithms and parallelization strategies, Fundamenta Informaticae 41.

[27] D. Sinha, P. Sinha, E. R. Dougherty, S. Batman, Design and analysis of fuzzy morphological algorithms for image processing, IEEE Transactions on Fuzzy Systems 5 (4) (1997) 570–583.

[28] P. Soille, Morphological Image Analysis, Springer Verlag, Berlin, 1999.

[29] P. Sussner, Lattice fuzzy transforms from the perspective of mathematical morphology, Fuzzy Sets and Systems 288 (2016) 115–128, special Issue on F-Transform: Theoretical Aspects and Advanced Applications.

[30] P. Sussner, L. C. Carazas, An approach towards image edge detection based on interval-valued fuzzy mathematical morphology and admissible orders, in: Proceedings of the 11th Conference of the European Society for Fuzzy Logic and Technology (EUSFLAT 2019), 2019/08, pp. 690–697.

[31] P. Sussner, M. Nachtegael, T. Mélange, G. Deschrijver, E. Esmi, E. Kerre, Interval-valued and intuitionistic fuzzy mathematical morphologies as special cases of $\mathbb{L}$-fuzzy mathematical morphology, Journal of Mathematical Imaging and Vision 43 (1) (2012) 50–71.

[32] P. Sussner, M. E. Valle, Classification of fuzzy mathematical morphologies based on concepts of inclusion measure and duality, Journal of Mathematical Imaging and Vision 32 (2) (2008) 139–159.

[33] Y. Vardi, L. Shepp, L. Kaufman, A statistical model for positron emission tomography, Journal of the American Statistical Association 80 (389) (1985) 8–20.

[34] L. Vincent, P. Soille, Watersheds in digital spaces: An efficient algorithm based on immersion simulations, IEEE Transactions on Pattern Analysis and Machine Intelligence 13 (6) (1991) 583–598.